Click Here for Full Article

Biogeochemical iron budgets of the Southern Ocean south of Australia: Decoupling of iron and nutrient cycles in the subantarctic zone by the summertime supply

Andrew R. Bowie,[1] Delphine Lannuzel,[1] Tomas A. Remenyi,[1] Thibaut Wagener,[2,3] Phoebe J. Lam,[4] Philip W. Boyd,[5] Cécile Guieu,[2] Ashley T. Townsend,[6] and Thomas W. Trull[1,7,8]

Received 22 February 2009; revised 15 July 2009; accepted 9 September 2009; published 31 December 2009.

[1] Climate change is projected to significantly alter the delivery (stratification, boundary currents, aridification of landmasses, glacial melt) of iron to the Southern Ocean. We report the most comprehensive suite of biogeochemical iron budgets to date for three contrasting sites in subantarctic and polar frontal waters south of Australia. Distinct regional environments were responsible for differences in the mode and strength of iron supply mechanisms, with higher iron stocks and fluxes observed in surface northern subantarctic waters, where atmospheric iron fluxes were greater. Subsurface waters southeast of Tasmania were also enriched with particulate iron, manganese and aluminum, indicative of a strong advective source from shelf sediments. Subantarctic phytoplankton blooms are thus driven by both seasonal iron supply from southward advection of subtropical waters and by wind-blown dust deposition, resulting in a strong decoupling of iron and nutrient cycles. We discuss the broader global significance our iron budgets for other ocean regions sensitive to climate-driven changes in iron supply.

Citation: Bowie, A. R., D. Lannuzel, T. A. Remenyi, T. Wagener, P. J. Lam, P. W. Boyd, C. Guieu, A. T. Townsend, and T. W. Trull (2009), Biogeochemical iron budgets of the Southern Ocean south of Australia: Decoupling of iron and nutrient cycles in the subantarctic zone by the summertime supply, *Global Biogeochem. Cycles*, *23*, GB4034, doi:10.1029/2009GB003500.

1. Introduction

[2] Iron (Fe) is known to limit primary productivity in high nutrient low chlorophyll (HNLC) regions globally, and in particular over vast regions of the Southern Ocean [e.g., *de Baar et al.*, 1995; *Sedwick et al.*, 1999; *Boyd et al.*, 2000]. Higher nutrient utilization efficiency of the ocean's biological pump (currently only ~50%) driven by elevated iron supply could have been partially responsible for reduced atmospheric carbon dioxide concentrations during the last ice age [*Watson et al.*, 2000]. Recent studies have debated the relative magnitude of different sources of iron to surface open Southern Ocean waters, including upwelling [*de Baar et al.*, 1995], dust delivery [*Boyd et al.*, 2004; *Cassar et al.*, 2007, 2008; *Boyd and Mackie*, 2008], entrainment from shelf sediments [*Blain et al.*, 2007], and advection of subtropical waters from the north [*Sedwick et al.*, 2008]. *Ellwood et al.* [2008] have shown that the main supply of dissolved iron (dFe) into the subantarctic zone (SAZ) south of Australia during winter is via Ekman transport of waters from the south. Iron-laden dust supply from Australia is also thought to stimulate regional Southern Ocean phytoplankton blooms [*Cassar et al.*, 2007; *Mackie et al.*, 2008]. A recent reevaluation of the importance of other iron supply mechanisms suggests that sedimentary resuspension and aerosols probably make similar global contributions [*Moore and Braucher*, 2008].

[3] One of the major unknowns in assessing the interactions of circulation, biogeochemistry, and ocean productivity in the Southern Ocean is the dependence of ecosystem structuring on differing natural iron supply mechanisms, resulting in varying degrees of microbial iron limitation [e.g., *Boyd et al.*, 2005; *Blain et al.*, 2007]. Despite widespread iron limitation in the modern HNLC Southern Ocean, intense algal blooms are observed annually, particularly in waters of the northern SAZ and in the subtropical front (STF) [*Boyd et al.*, 1999]. In particular, the Southern Ocean south of Tasmania (Australia) is conspicuous in

[1]Antarctic Climate and Ecosystems CRC, University of Tasmania, Hobart, Tasmania, Australia.
[2]Laboratoire d'Océanographie de Villefranche sur Mer, Université Pierre et Marie Curie, Villefranche sur Mer, France.
[3]Now at Marine Biogeochemie, Chemische Ozeanographie, Leibniz-Institut für Meereswissenschaften an der Universität Kiel, IFM-GEOMAR, Kiel, Germany.
[4]Department of Marine Chemistry and Geochemistry, Woods Hole Oceanographic Institution, Woods Hole, Massachusetts, USA.
[5]NIWA Centre for Chemical and Physical Oceanography, Department of Chemistry, University of Otago, Dunedin, New Zealand.
[6]Central Science Laboratory, University of Tasmania, Hobart, Tasmania, Australia.
[7]CSIRO Marine and Atmospheric Research, Hobart, Tasmania, Australia.
[8]Institute of Antarctic and Southern Ocean Studies, University of Tasmania, Hobart, Tasmania, Australia.

Copyright 2009 by the American Geophysical Union.
0886-6236/09/2009GB003500$12.00

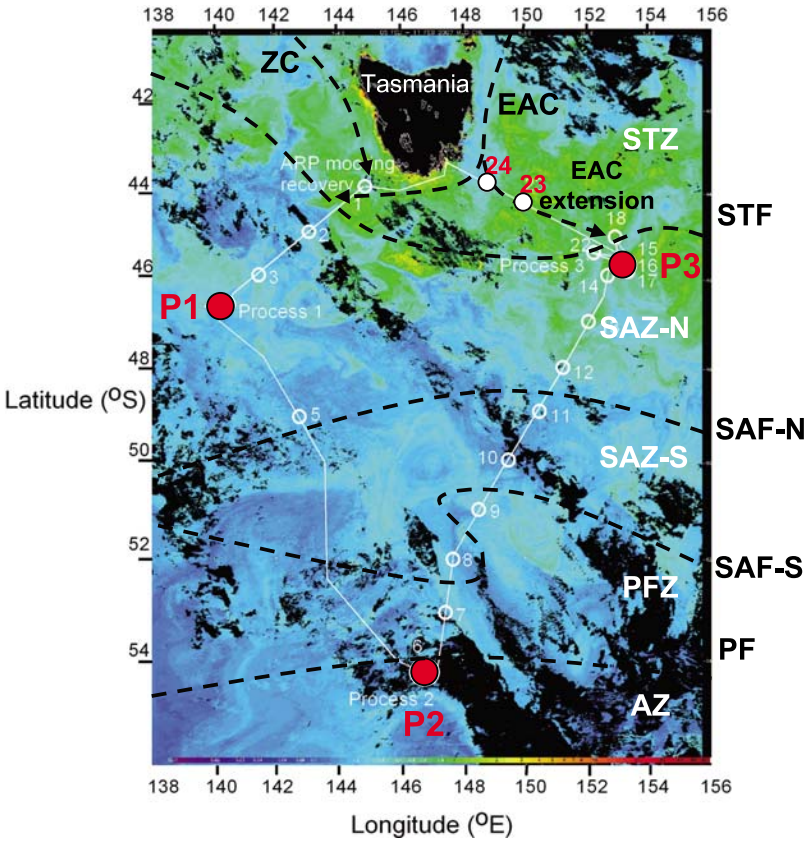

Figure 1. SAZ-Sense voyage track and station locations superimposed on ESA Meris satellite ocean color composite image from 5 to 11 February 2007. Process stations are shown as red dots (P1, SAZ-west; P2, PF; P3, SAZ-east), and stations 23 and 24 on the transect from P3 to Tasmania are shown as solid white dots. Approximate locations of currents (EAC, East Australian Current; ZC, Zeehan Current) and fronts in summer are shown (STF, subtropical front; SAF-N, subantarctic front north; SAZ-S, subantarctic front south; PF, polar front), separating distinct water masses (STZ, subtropical zone; SAZ-N, subantarctic zone north; SAZ-S, subantarctic zone south; PFZ, polar frontal zone; AZ, antarctic zone). The north-south and east-west gradients in phytoplankton chlorophyll biomass are typical of the region in summer. Satellite image processing by Plymouth Marine Laboratory Remote Sensing Group.

having large differences in surface water productivity and biomass between sectors east and west of Tasmania, and between subantarctic and polar waters [*Trull et al.*, 2001] (Figure 1). The region southwest of Tasmania (135–145°E) is typical of much of the circumpolar SAZ and exhibits relatively low phytoplankton biomass, in contrast to the higher biomass region to the southeast of Tasmania (150–160°E), where subtropical waters mix into the SAZ (M. Mongin, personal communication, 2009). Atmospheric and ocean circulation changes driven by climate warming may cause the SAZ to experience greater inputs from strengthening subtropical gyres, such as those that reach the region east of Tasmania today in East Australian Current (EAC) eddies, and thus the circumpolar SAZ may become more like this region in the future [*Hill et al.*, 2008; *Ridgway*, 2007a; *Ridgway and Dunn*, 2007]. Indeed chlorophyll concentrations, derived from satellite, have been observed to increase in the SAZ region southeast of Australia during the last decade (M. Mongin, personal communication, 2009). Subantarctic waters also have global importance as a sink for anthropogenic carbon dioxide and as a site for subduction of oxygenated nutrient-rich waters beneath the subtropical gyres [*Metzl et al.*, 1999]. It is therefore imperative that we assess the controls on these spatial differences in phytoplankton biomass and productivity in the SAZ in order to understand how such processes are evolving on decadal to centennial timescales.

[4] A study of SAZ waters east, west and south of Tasmania represents an excellent approach to examine biogeochemical cycling in the Southern Ocean, because it can address the effects of persistent, varying and multiple iron sources that are not accessible through deliberate mesoscale iron fertilization experiments. The interaction of these waters with several circumpolar fronts of the broader Southern Ocean further south also allows us to place our regional observations within a global context. Since iron is actively taken up into phytoplankton, and transferred throughout the food web, including removal by particle settling and remineralization in deep waters, the assessment of its availability is complex and cannot be

assessed from dissolved iron levels in surface waters alone. Only one other study (FeCycle) has concurrently measured iron associated with different phases (dissolved and particulate), and quantified iron export losses in concert with vertical and lateral advective iron supply [*Boyd et al.*, 2005; *Frew et al.*, 2006]. This paper reports the results of a specific oceanographic study termed SAZ-Sense (''Sensitivity of the subantarctic zone to environmental change'') carried out in the SAZ and polar frontal zone (PFZ) south of Australia in mid-to-late austral summer (21 January to 19 February 2007), and presents biogeochemical iron budgets, focusing on sources of new iron and on iron sinks, for process stations at three contrasting regions of the Southern Ocean. We report measurements of dissolved iron gradients across the seasonal pycnocline to estimate fluxes from below, high resolution horizontal gradients coupled with tracer release modeling simulations to estimate large scale advective iron inputs, aerosol observations to estimate atmospheric iron supply, and free-floating sediment trap fluxes to estimate iron export. Our budget uses ^{55}Fe and ^{14}C as radiotracers of phytoplankton uptake rates and heterotrophic bacterial remineralization, iron-to-carbon (Fe/C) uptake and export ratios, and reports measurements of other ''fingerprint'' particulate trace elements (i.e., aluminum and manganese) that confirm the provenance of iron supplied from dusts and shelf sediments. We place our seasonal iron budgets within the context of the broader SAZ-Sense biogeochemical observations to examine the relationship between iron and major nutrients, the carbon sequestration efficiency with respect to iron supply, *f*e (uptake of new iron/uptake of new + regenerated iron) and F*e* (biogenic iron export/uptake of new + regenerated iron) ratios [*Boyd et al.*, 2005], and compare predicted versus observed primary productivity based on iron availability.

2. Methods

[5] All trace metal sampling and analytical procedures followed recommended GEOTRACES protocols as closely as possible [*Bowie and Lohan*, 2009], and are detailed in Text S1.[1] Dissolved iron data were quality controlled against the SAFe reference samples [*Lannuzel et al.*, 2009].

2.1. Oceanographic Setting

[6] The SAZ-Sense study targeted a diamond-shaped grid in the Australian sector of the Southern Ocean south of Tasmania (Figure 1), with waters ranging from subtropical through subantarctic to polar. The area is characterized north-to-south by several circumpolar fronts [*Trull et al.*, 2001] (Figure 2). The SAZ region southeast of Australia is also strongly influenced by mixing with subtropical water from the north and from the EAC extension traveling south along the Tasmanian shelf break. The deeper water masses observed in our study region included subantarctic mode water (SAMW), antarctic intermediate water (AAIW) and upper circumpolar deep water (UCDW). SAMW formed by deep winter convection (to 600 m) north of the SAF can be traced north to 38°S in the Tasman Sea [*Sokolov and Rintoul*, 2003]. In summer, there is a cap of warmed water overlying the SAMW. In the southern SAZ, cool, fresher water formed by isopycnal advection across the SAF spreads north via Ekman transport [*Rintoul and Trull*, 2001]. Poorly ventilated AAIW is found below SAMW north of the SAF and is defined by a prominent salinity minimum at 700–1100 m [*Rintoul and Bullister*, 1999].

[7] Process station 1 (P1, 140.6°E, 46.3°S) was located in northern SAZ waters ~530 km southwest of Tasmania (SAZ-West station). Below the 53 m mixed layer, there was active lateral mixing with high salinity, subtropical water from the north (50–200 m depth range; Figure 3d) which may have been influenced by southward penetration of the Leeuwin and Zeehan currents which travel east along the south coast of Australia and then divert south along the Tasmanian west coast [*Ridgway*, 2007b]. SAMW was identified between 250 and 600 m. Process Station 2 (P2, 145.9°E, 54.0°S) was located ~1150 km directly south of Tasmania in polar front (PF) waters (PF station), as indicated by the presence of a T_{min} layer between 100 and 250 m (<2°C, indicative of remnant winter waters) below the 52 m mixed layer (Figure 3e), and underlying a deep chlorophyll maximum at 60–100 m. No SAMW was identified deeper in the water column. Process Station 3 (P3, 153.2°E, 45.5°S) was located ~480 km southeast of Tasmania in an extremely dynamic region at the very northernmost edge of the SAZ (SAZ-East station), and was strongly influenced by the lateral mixing of warm salty subtropical water (influenced by eddies of the EAC extension) with cooler fresh SAZ water [*Ridgway*, 2007b]. This complex mixing resulted in high and variable surface chlorophyll *a* concentrations (Figure 1). The STF was present as a broad feature covering several degrees of latitude with the southern edge just north of P3 at 45.5°S. We observed significant differences in salinity, nitrate and phosphate concentrations in the different layers in the upper 125 m at P3 (and also between different station casts over our 1 week occupation), which reflects the complexity of the region. Two surface mixed layers were present, a shallow stratified feature ~16 m deep overlying a deeper seasonal mixed layer ~70 m thick (Figure 3f). SAMW was present between 300 and 400 m, but was less oxygenated at P3 than the SAMW at P1, and AAIW was defined by a salinity minimum near 1000 m.

[8] Stations along the northeast ''return'' transect from P3 to Tasmania were all in EAC/subtropical waters with surface salinities >35.4 and temperatures >16°C. Several filaments of the EAC and STF and other minor fronts were crossed on this northeast transect, again reflecting the complex ocean mixing in the region. Southward penetrating waters of the EAC extension and Tasman Sea traveled along the east coast of Australia before surface waters mostly separated from the Tasmanian coast and flowed eastward upon mixing with subantarctic waters (Figure 1). Some deeper (500–1200 m) waters also flowed westward during summer around southern Tasmania via the Tasman Outflow [*Ridgway*, 2007b], providing a link between the EAC and Indian Ocean [*Ridgway and Dunn*, 2007]. The surface waters that tended to be diverted east then traveled northeast toward P3. Geostrophic velocity analyses derived from satellite altimetry observations (M. Mongin, personal com-

[1] Auxiliary materials are available with the HTML. doi:10.1029/2009GB003500.

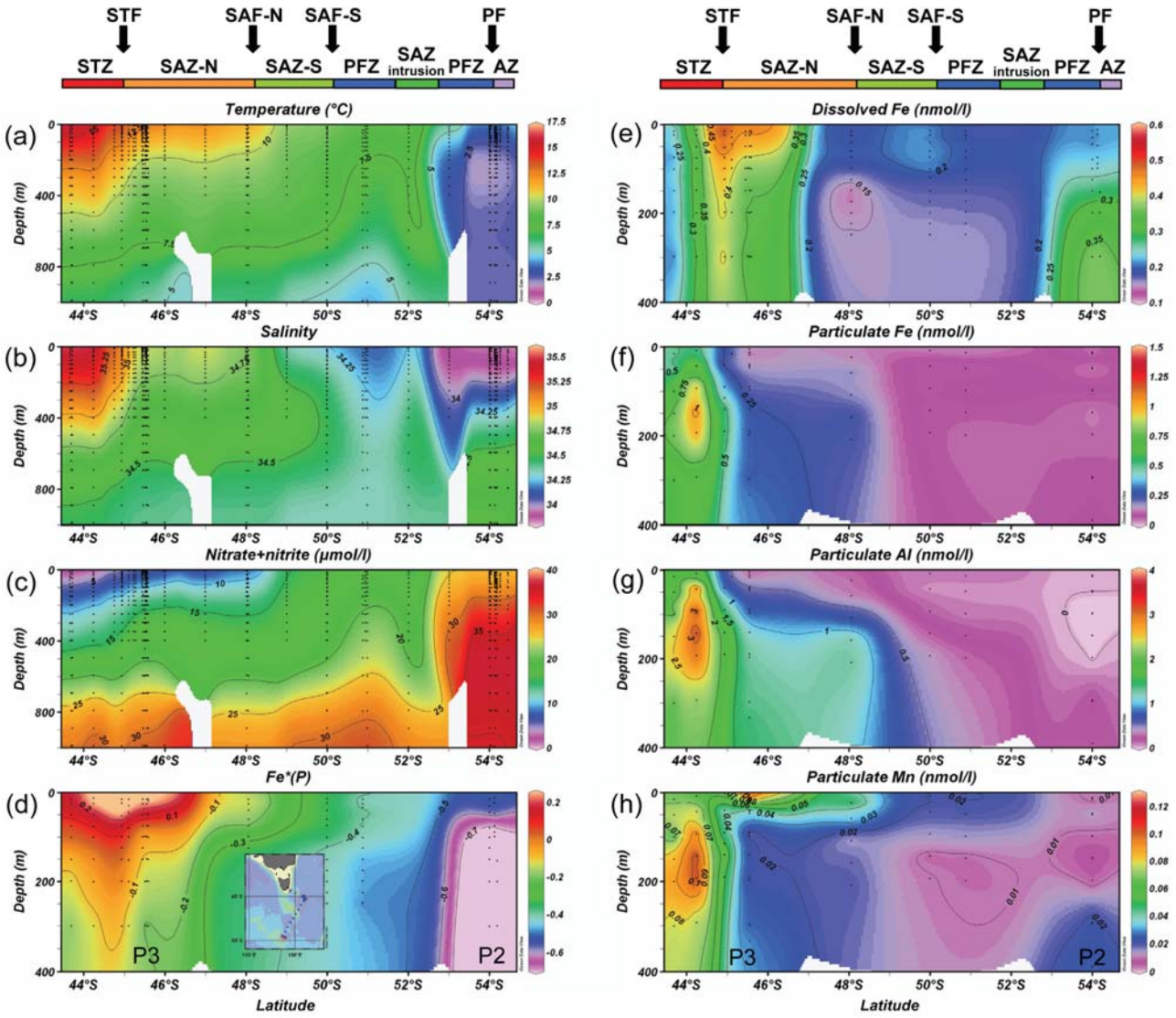

Figure 2. (a) Temperature, (b) salinity, (c) nitrate+nitrite in the upper 1000 m, and (d) Fe*(P) (defined as Fe*(P) = [dFe] − {(Fe/P) algal uptake ratio × $[PO_4^{3-}]$}; see section 3.3), (e) dissolved iron, (f) particulate iron, (g) particulate aluminum, and (h) particulate manganese in the upper 400 m along the southeast-northeast section from P2 to P3 to Tasmania (shown as inset in Figure 2d). The positions of oceanographic fronts and zones are indicated. Note the difference in the depth scales in Figures 2a–2c compared to Figures 2d–2h. Prepared using Ocean Data View (R. Schlitzer, http://odv.awi.de).

munication, 2009) indicate that this EAC-influenced water traveled further offshore and east of our last transect station 24 (148.6°E, 43.7°S), ~70 km southeast of Tasmania.

2.2. Dust Deposition and Atmospheric Circulation Over the Studied Area

[9] The transport of dust from the Australian continent to the Tasman Sea and Southern Ocean has been documented through marine sedimentary observations [*Hesse*, 1994] or from atmospheric sampling in New Zealand (*McGowan et al.* [2005]; see review by *Mackie et al.* [2008]). Although episodic and spatially variable, the maximum of mineral dust transport from the Australian continent occurs in the austral spring and summer [*Ekstrom et al.*, 2004; *Boyd et al.*, 2004; *Mahowald et al.*, 2005]. The greatest bushfire activity also occurs during these months, which may provide an additional and more soluble source of iron to the ocean, either directly [*Guieu et al.*, 2005; *Luo et al.*, 2008; *Schroth et al.*, 2009], or via merging of dust and biomass-burning aerosols due to enhanced atmospheric processing in the presence of higher major ion (NO_x, SO_x) concentrations in smoke (D. Mackie, personal communication, 2008). Thus the SAZ-Sense cruise occurred during the period of annual maximum Australian aerosol supply, although general atmospheric circulation patterns suggest that dust should preferentially be transported to the east of Australia (i.e., north of P3) at this time [*Ekstrom et al.*, 2004]. Air mass

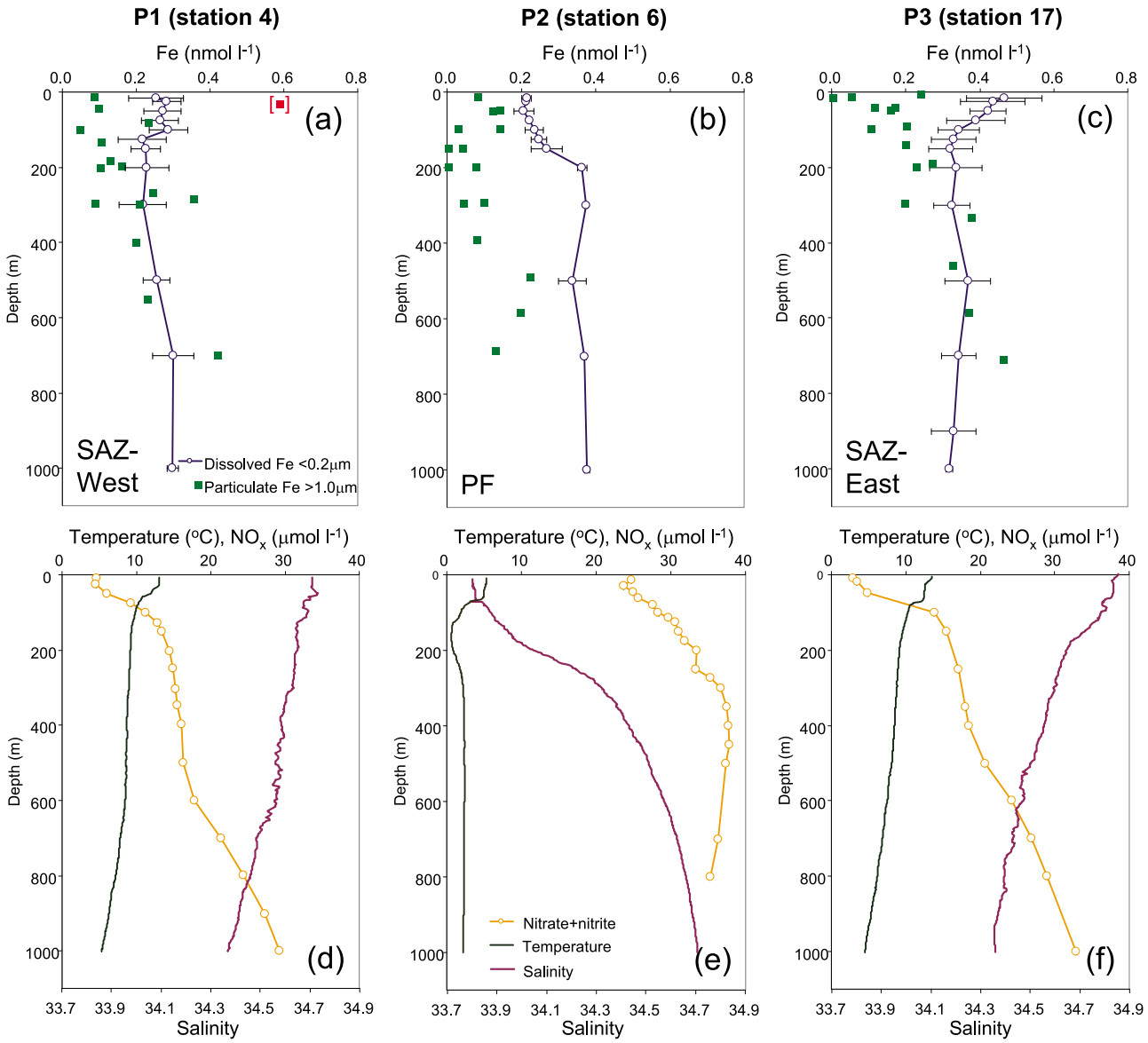

Figure 3. Vertical profiles of dissolved and particulate iron, temperature, salinity, and nitrate+nitrite at our three process stations in the SAZ-West (P1), PF (P2), and SAZ-East (P3). The dFe data represent the mean ±1 standard deviation of independent casts (n = 3–4) at each process station over the period of ~1 week and include analytical uncertainty (~7%) and uncertainty due to sampling and "real" variability (spatial and temporal) (up to 30%). The pFe data represent individual data points for each separate deployment of the McLane in situ pumps (n = 2–3). The pFe errors bars averaged 15% on the basis of the independent digestion and analysis of replicate (n = 2) subsample punches taken from the same filter. The pFe data were scattered somewhat through the water column, which is typical for particulate trace metals. Red data point in square brackets at 32 m depth at P1 in Figure 3a is possibly contaminated.

back trajectory calculations using the HYSPLIT model (see Text S1 and Figure S1) over the period 2004 to 2007 indicated that only dust of Australian origin was able to enrich air masses transported over the region sampled during the SAZ-Sense cruise. These back trajectory calculations did not demonstrate significant differences in the frequency of air masses originating from Australian dust sources between eastern (P3) and the western (P1) SAZ sectors, whereas the frequency was significantly lower for polar waters further south (P2) (t test, n = 852, P = 0.05). Back trajectories for each day of the cruise indicated that sampled air masses originated from marine sources and not Australia (Figure S1). For stations situated north of 45°S, the trajectories had a higher probability of originating from a northeast sector, whereas for stations situated south of 45°S, air masses likely originated from open Southern

Ocean waters, with characteristic west-to-east long distance circulation.

3. Results and Discussion

3.1. Dissolved Iron Distributions

[10] We observed significant variation in mixed layer dFe concentrations (~0.1–0.7 nmol L^{-1}) between the 19 different trace metal stations occupied in the study region (locations shown in Figure S2; data reported by *Lannuzel et al.* [2009]). In general, mean mixed layer dFe concentrations decreased from north-to-south, and were highest at the SAZ-East station (P3, 0.45 nmol L^{-1}; range 0.37–0.58 nmol L^{-1}), intermediate at the SAZ-West station (P1, 0.33 nmol L^{-1}; range 0.20–0.31 nmol L^{-1}) and lowest at the PF station (P2, 0.21 nmol L^{-1}; range 0.19–0.23 nmol L^{-1}) (Figures 3a–3c), and were significantly different at each process station (*t* test, $P = 0.05$). In principle, this could reflect either: (1) different winter reserve dFe concentrations, (2) spatial variability in biomass and hence Fe uptake, or (3) different sources (upwelling, lateral advection, dust deposition) and magnitude of the dFe supply terms. Since *Ellwood et al.* [2008] have shown that wintertime dFe reserves in the SAZ (between 155 and 160°E, 40–52°S) are lower than our summertime observations, and productivity was similar at stations P1 and P3 and greater than station P2 (Table 1) during SAZ-Sense, we conclude that the differences in surface dFe concentrations were probably derived from differing iron sources to the three process stations. Deep water dFe concentrations (1000 m) were remarkably consistent at all 19 stations (0.25–0.37 nmol L^{-1}), and lower than reported in the Atlantic and Pacific basins (0.6–0.8 nmol L^{-1}) [*Johnson et al.*, 1997]. This indicates that supply of waters from below (through either seasonal winter overturning and deepening of the mixed layer, or episodic short-term events such as storms) will not provide a significant amount of dFe to the mixed layer in the SAZ, and implicates lateral advection or atmospheric inputs as important sources to SAZ surface waters in summer.

[11] We observed distinctly different dFe profiles at each process station (Figures 3a–3c), although good linear correlations between the vertical distributions of dFe and salinity in the upper 200 m at all three sites highlighted the importance of upper ocean internal mixing in controlling dFe distributions. At P1 (SAZ-West), elevated dFe concentrations in the mixed layer (0.33 nmol L^{-1}) decreased to 0.22 nmol L^{-1} between 125 and 300 m, and increased again to 0.30 nmol L^{-1} down to 1000 m (Figure 3a). At P2 (PF), we observed a nutrient-like profile with a ferricline located at a depth stratum of about 150–200 m, ~100 m shallower than the nitracline. The nutrient-like vertical profile and depth of the ferricline indicated that colder, saltier upwelled deep waters were the primary dFe source (Figures 2b, 2e, 3b, and 3e and Table 1), but also showed that relative rates of dFe and NO_x remineralization were different. At P3 (SAZ-East), elevated dFe concentrations in the mixed layer (0.45 nmol L^{-1}) decreased gradually to 0.3 nmol L^{-1} at 150 m and were relatively uniform below this depth (Figure 3c). Elevated mixed layer dFe concentrations at P3 coincided with warmer, saltier and low nitrate waters that had been advected from the north (Figures 2a–2c). Interestingly, the section along our southeast-northeast transect from P2 to P3 and then back to Hobart (Figure 2e) showed that elevated dFe concentrations tended to be focused in 0–200 m depth range in the band of water at the northern SAZ and in the STF, with lower dFe concentrations further northwest in subtropical waters closer to Tasmania (stations 23 and 24), probably due to the passage of EAC-influenced waters further offshore [*Ridgway*, 2007a; M. Mongin, personal communication, 2009]. This pattern differs to the distributions of particulate trace metals, which were elevated closer to the Tasmania (see section 3.2). North of the PF and in the broader SAZ between 47.0 and 52.5°S, dFe concentrations were slightly higher in the upper 100 m than in the 150 m depth stratum immediately below (no data available below 250 m), perhaps reflecting the summertime supply of atmospheric iron [*Cassar et al.*, 2007].

[12] Our range of dFe concentrations is broadly consistent with historical data for the region [*Sedwick et al.*, 1997, 1999, 2008; *Bowie et al.*, 2004; *Sohrin et al.*, 2000], noting that the majority of previous measurements were only made to 300 m depth and no previous summertime iron data coverage exists to the southeast of Tasmania. The wintertime surface SAZ data of *Ellwood et al.* [2008] are generally lower (by ~0.1 nmol L^{-1}) than our observations and their deep (1000 m) data higher (by ~0.1–0.2 nmol L^{-1}), which implies that iron sources to the Australian SAZ region are strongly dependant on season and location, and biological iron uptake and remineralization processes were not the dominant factors controlling distributions in summer. Since both this study and *Ellwood et al.* [2008] employed surface (S1) and deep (D2) SAFe standards, we believe a direct comparison is robust. It also appears that direct deposition of soluble Fe in atmospheric dust was of less importance in the SAZ (see section 3.4) than the earlier FeCycle study to the southeast of New Zealand [*Boyd et al.*, 2005], although longer-range transport of warm and salty waters from the north (which may have been enriched with iron from dust transported east of Australia) may have occurred prior to our occupation at P3. Both the high dFe concentrations and the possibility of long-range oceanic transport are consistent with the observed iron(III)–organic ligand concentrations (L) which were greatest in surface waters and always exceeded the dFe concentration (L/dFe > 1.5), and thus sufficient to keep dFe in solution and potentially bioavailable [*Ibisanmi et al.*, 2009].

3.2. Particulate Iron, Aluminum, and Manganese Distributions

[13] Particulate iron (pFe) concentrations were generally lower than dFe at all three process stations (Figures 3a–3c), with no clear evidence of surface enrichment driven by atmospheric dust supply that our surface dFe data at the SAZ-East station (P3) may have suggested. We observed slightly higher pFe values at depths below 190 m at station P3. Higher subsurface concentrations for particulate aluminum (pAl), manganese (pMn) and iron (up to 1.4 nmol L^{-1}) were observed in subtropical waters on the northeast transect between P3 and Hobart (Figures 2f–2h). The depth stratum and spatial extent of the subsurface maxima (40–200 m) suggests an internal advective source from Tasmanian or eastern mainland Australian shelf sediments, or

Table 1. Summary of Iron Pools and Fluxes for the Surface Mixed Layer at Each of the SAZ-Sense Process Stations During Summer

Property[a]	Process Station 1 (P1)	Process Station 2 (P2)	Process Station 3 (P3)
Region	SAZ-West	PF	SAZ-East
Mixed layer depth[b] (m)	53	52	70
	Pools[c]		
dFe	14 ± 2	11 ± 1	31 ± 5
pFe	4 ± 1	6 ± 2	7 ± 5
POC (mmol m^{-2})	152 ± 110	101 ± 18	575 ± 436
	Fluxes[d]		
(a) Vertical diffusive dFe supply[e]	−2 ± 0	7 ± 1	−31 ± 5
(b) Vertical advective dFe flux[f]	Negligible	47	Negligible
(c) Lateral advective dFe supply[g,h]	67 ± 22 (range: 48–91)	24 ± 7 (range: 17–31)	124 ± 53 (range: 85–191)
(d) Atmospheric total iron deposition[i]	488 ± 386	288 ± 180	354 ± 212
(e) Atmospheric dFe deposition[i]	2.4 ± 2.1	4.0 ± 3.2	7.4 ± 4.3
(f) Downward pFe export flux	166 ± 89	69 ± 14	213 ± 51
(g) Downward POC export (μmol m^{-2} d^{-1})	3339 ± 1805	2114 ± 884	858 ± 382
(h) Iron uptake[j]	5842 ± 537	1825 ± 242	4062 ± 518
(i) Iron remineralization[k]	1206 ± 259	261 ± 124	977 ± 139
	Fe/C Ratios[l]		
(j) Mixed layer Fe/C cellular uptake ratio[m]	70 ± 44	60 ± 9	74 ± 47
Suspended mixed layer particulate Fe/C ratio	40 ± 31	55 ± 14	32 ± 30
Sinking Fe/C export ratio	50 ± 38	33 ± 15	248 ± 125
	Iron Supply Versus Demand[n]		
Total iron supply from "new" sources[o] [a+b+c+d]	553 ± 387	366 ± 180	447 ± 219
Additional iron requirement to balance the budget[p] [a+b+c+d−f−h+i]	−1836 ± 716	−744 ± 326	−915 ± 582
(k) Biological uptake of "new" iron[q] [a+b+c+d−f]	387 ± 397	297 ± 181	234 ± 224
*f*e ratio[r] [k/h]	0.07 ± 0.07	0.16 ± 0.10	0.06 ± 0.06
F*e* ratio[r] [f/h]	0.03 ± 0.02	0.04 ± 0.01	0.05 ± 0.01
	Estimated Versus Observed Production[s]		
Potential new primary production [k/j][t]	5.5 ± 6.6	5.0 ± 3.1	3.2 ± 3.7
Observed gross primary production[u]	108.7 ± 25.0	39.6 ± 14.1	62.4 ± 45.3

[a]The letters in parentheses refer to each different property in the budget and indicate how the calculations were performed under "iron supply versus demand" and "estimated versus observed production" (e.g., total iron supply from "new" sources = [a+b+c+d]).

[b]Defined from density profiles as the first depth below 10 m deep where $[\sigma - \sigma_{(10\ m)}] > 0.05$ [*Rintoul and Trull*, 2001], except at P3 where a shallower stratified mixed layer was also identified at 16 m so the mixed layer was based on Brunt-Väisälä frequency.

[c]Units are μmol m−2, unless otherwise stated.

[d]Units are nmol m^{-2} d^{-1}, unless otherwise stated.

[e]The vertical diffusive supply was derived from the dFe gradients across the pycnocline and a K_z of 0.66 ± 0.11 cm^2 s^{-1} for FeCycle [*Croot et al.*, 2007] which covers the range for the Southern Ocean [*Boyd et al.*, 2005]; a negative value indicates an iron loss from the mixed layer.

[f]Upwelling at P2 defined as vertical velocity (0.13 m d^{-1} [*de Baar et al.*, 1995]) × deep dFe concentration; includes contribution from remineralization.

[g]Estimated from the Bluelink model using a tracer release simulation for iron with a conservative 3% decay rate (i.e., accounting for biological uptake and scavenging) over 5 months using mean annual mixed layer depths at each process station (46 m at P1 and P3, and 53 m at P2); includes contribution from shelf sediments and advected dust; the reported ranges represent the theoretical lower and upper limits based on 0% and 7% decay rates for the advected dust (M. Mongin, personal communication, 2009).

[h]Although *Ellwood et al.* [2008] calculated a summertime flux of 43 μmol m^{-2} d^{-1} to the SAZ from Ekman-driven lateral advection from the south, our observed dFe concentration in source waters associated with this flux is low thus tending to result in no net increase in surface dFe concentrations through lateral transport.

[i]Fluxes for station P1 estimated from aerosol sample AeroSAZ-1, for station P2 from aerosol sample AeroSAZ-3, and for station P3 from aerosol samples AeroSAZ-6 and AeroSAZ-7.

[j]Column integrals for iron uptake by phytoplankton >0.2 μm, calculated using Simpson's rule.

[k]Column integrals for remineralization based on bacterial mobilization of algal iron within cells >5 μm (extrapolated to >0.2 μm using ratio of uptake-to-remineralization) calculated using Simpson's rule. This will underestimate remineralization by 3–4 fold as it does not include that due to bacterivory and herbivory [*Strzepek et al.*, 2005; P. W. Boyd et al., Remineralization of upper ocean particles: Implications for iron biogeochemistry, submitted to *Limnology and Oceanography*, 2009]. Microzooplankton grazing at all three sites accounted for most of daily primary production [*Pearce et al.*, 2009], indicating that iron remineralization rates were comparable to iron uptake rates observed during FeCycle by *Strzepek et al.* [2005].

[l]Units are μmol/mol.

[m]Mean mixed layer values and standard deviation. Note these values are notably higher than those reported for iron-limited conditions during SOFeX [*Twining et al.*, 2004] and those inside the KEOPS bloom [*Sarthou et al.*, 2008], but comparable to SOFeX iron replete conditions (also see the synthesis on Fe/C ratios reported by *Boyd et al.* [2007, Figure 3] and *de Baar et al.* [2008, Table 2]).

[n]Units are nmol m^{-2} d^{-1}.

[o]Assumes all the total iron atmospheric supply is available (see section 3.6).

[p]A negative value indicates an additional iron requirement.

[q]Compares well with the estimated biological requirement from "new" iron sources predicted for the SAZ by *Ellwood et al.* [2008] (250–410 nmol m^{-2} d^{-1}).

[r]F*e* is biogenic iron export/uptake of new + regenerated iron and *f*e is uptake of new/uptake of new + regenerated iron [*Boyd et al.*, 2005]. Note the *f*e and F*e* ratios would be considerably underestimated if these calculations did not include the total iron fraction in atmospheric dust (our calculated solubilities range from 0.2 to 2.5% for SAZ-Sense, excluding sample AeroSAZ-8; see Table S1) and noting the uncertainties on the lithogenic versus biogenic fraction of exported particulate iron (see section 2).

[s]Units are mmol C m^{-2} d^{-1}.

[t]Calculated using the biological uptake of "new" iron (k) and molar Fe/C cellular uptake ratio (j).

[u]Gross primary productivity in the mixed layer taken (K. Westwood, personal communication, 2009); data compare well to 24 h dual-labeled ^{14}C radiotracer incubation experiments.

advected dust (i.e., the transport and lateral advection of Australian dust initially deposited in distant ocean waters north of the SAZ-Sense region), rather than direct (local) atmospheric deposition. This trace metal-enriched feature at depth is also consistent with a saltier, slightly warmer and less oxygenated intrusion of waters between 100 and 250 m, evident from the individual depth profile at station 23 (Figure S3). This indicates that these subsurface waters are enriched with pFe, pAl and pMn from waters which have interacted with suboxic shelf-edge sediments. It is interesting to note that this subsurface feature does not correspond to a dFe maximum, indicating a decoupling of dFe and pFe. Rather, dFe is elevated further offshore and entrained in the STF around P3 at ~45°S, particularly in surface waters down to ~100–200 m (Figure 2e). Two plausible explanations for this trend are that either the dFe feature results from a different source (e.g., dust deposition rather than resuspended sediments) or that pFe is slowly solubilized (on timescales of weeks to months, according to tracer release model simulations (M. Mongin, personal communication, 2009)), as waters are gradually advected south and to the east. This process may be driven by microbial solubilization of biogenic pFe and/or coupled microbial/photochemical dissolution of lithogenic pFe [*Boyd et al.*, 2005]. Clearly, P3 was located in an extremely complex and dynamic region where HNLC subantarctic waters mixed with iron-rich subtropical waters in the presence of a series of complex eddies (originating from the EAC extension [*Ridgway*, 2007a]) that had interacted with the shelf-edge on their 3–6 month southerly passage along the east coast of Australia (M. Mongin, personal communication, 2009). Our suspended particulate trace metal data compares reasonably well with the few published profiles in Southern Ocean waters [*Sarthou et al.*, 1997; *Fitzwater et al.*, 2000; *Coale et al.*, 2005; *Frew et al.*, 2006], tending to be at the lower end of the reported ranges.

3.3. Iron and Major Nutrients

[14] Surface nitrate and phosphate concentrations increased southward from the STF to the PF and with depth (Figure 2c, only nitrate + nitrite shown). Northern SAZ waters (stations P1 and P3) showed a greater vertical gradient at the nitracline than waters in the PF (station P2) (Figures 3d–3f), due to surface depletion in these higher phytoplankton waters (Figure 1). In the PF, the nitracline was located at a greater depth than the ferricline. Silicic acid was depleted (<1 μmol L^{-1}) in surface waters over much of the study region, although there were appreciable reserves in deep waters of the HNLC PFZ and AZ (up to 80 μmol L^{-1}). The ratio of dissolved iron to nitrate + nitrite (dFe/NO_x) in our study region ranged over two orders of magnitude, from 1.7 mmol/mol in surface northern SAZ waters decreasing to 0.0075 mmol/mol in mixed layer PF waters. dFe/NO_x ratios at 1000 m depth were remarkably consistent at ~0.01 mmol/mol. The lower end of our range of dFe/NO_x data are consistent with ratios reported for FeCycle during summer (~0.01 mmol/mol) [*Croot et al.*, 2007], and the SAZ southwest of New Zealand during winter (0.005–0.032 mmol/mol) [*Ellwood et al.*, 2008]. dFe/NO_x ratios of ~0.01 mmol/mol are also consistent with studies in the HNLC North Pacific [*Martin et al.*, 1989]. In contrast, however, our higher dFe/NO_x data for surface waters of the SAZ do show that this ratio is seasonally variable and that there is an inherent difference between dFe and major nutrients dynamics in northern SAZ waters. Although differential remineralization length scales and phytoplankton consumption rates of dFe versus NO_x (driven by elevated Fe supply) will result in varying dFe/NO_x ratios [*Frew et al.*, 2006; *Ellwood et al.*, 2008], the main driver of the observed high ratios in the SAZ-Sense region is the delivery of iron-rich advected waters or atmospheric dust from the north in STZ and northern SAZ waters (both of which tend to be low in NO_x). These processes impact on iron distributions over short periods (days-to-weeks), and effectively decouple iron from the seasonal cycles of convective mixing, biological uptake and remineralization that are typical of major nutrients. Biological removal will not increase dFe/NO_x significantly until very large amounts (of the order of 90%) of the initial nitrate pool have been removed, which is uncommon in the SAZ, for which seasonal removal is typically close to 65% [*Lourey and Trull*, 2001].

[15] At P2, we observed a close coupling between iron and major nutrients in the PF (Figures 3b and 3e), with community consumption ratios (based on dissolved nutrient constituents) of dFe/NO_x = 15 μmol/mol, dFe/PO_4 = 170 μmol/mol and $Fe/Si(OH)_4$ = 2.2 μmol/mol. This equates to Fe/C uptake ratios of 1.6–2.3 μmol/mol (assuming Redfield C/N/P stoichiometry), and implying phytoplankton are iron-stressed in the PF (based on a minimum metabolic requirement of ~10 μmol/mol for iron-limited algal cultures [e.g., *Maldonado and Price*, 1996]. Iron supply from below is insufficient to significantly raise dFe/NO_x ratios and thus an additional iron input is required to relieve limitation in the PF. Interestingly, P. Ralph et al. (personal communication, 2009) observed a relatively high surface F_v/F_m ratio of 0.58 (using PhytoPAM) at this site which implies that the resident phytoplankton were not significantly nutrient-stressed, consistent with a surface dFe concentration of 0.2 nmol dFe L^{-1} (threshold for increased F_v/F_m during SOIREE was ~0.2 nmol L^{-1}) [*Boyd et al.*, 2000].

[16] Our calculated Fe/C uptake ratios based on dissolved nutrient budgets at P2 (above) are significantly lower than measured mixed layer Fe/C cellular uptake ratios from radiotracer experiments (60 ± 9 μmol/mol; Table 1). This may be a result of a deviation from nutrient stoichiometry and a lower uptake of iron relative to carbon at this site (see section 3.7), noting the possibility of variable uptake ratios and the difficulty in comparing nutrient stocks across pools that reflect changes on different timescales. Fe/C uptake ratios were also more variable at P1 and P3 compared to P2 (Table 1), which may reflect a more dynamic Fe demand in the northern SAZ due to changes in environmental forcings (e.g., light or silicic acid) [*Hoffmann et al.*, 2008]. The SAZ-Sense Fe/C radiotracer uptake ratios are similar to, although slightly higher than, the intracellular ratios observed in diatoms collected during SoFeX (9–48 μmol/mol) [*Twining et al.*, 2004]. Our observations indicate that luxury uptake was not an important process in the PF (based on Fe/NO_x) or the SAZ (based on $^{55}Fe/^{14}C$), so Redfield C/N/Fe stoichiometry appears valid.

[17] The tracer Fe* has been applied in recent studies [*Parekh et al.*, 2005; *Boyd et al.*, 2007; *Blain et al.*, 2008] to estimate the relative magnitude of iron versus macronutrient supply. This simple concept is based on the decoupling of iron and macronutrients (e.g., PO_4^{3-} or $Si(OH)_4$) through the water column due to scavenging of iron. Fe*(P) is thus defined as Fe*(P) = [dFe] – {(Fe/P) algal uptake ratio × $[PO_4^{3-}]$}, which subtracts the contribution of biological iron consumption from the dFe distribution to reveal the balance between advected and scavenged iron, following a method similar to that of N* [*Gruber and Sarmiento*, 1997]. A positive Fe*(P) implies that there is sufficient iron to support the complete consumption of PO_4^{3-} and primary production is ultimately macronutrient limited. A negative Fe*(P) implies there is a deficit and production is ultimately iron limited. The same concept applies to Fe*(Si), which is based on the relative abundance of iron to the reference macronutrient silicic acid. We have applied the tracer Fe*(P) along our section from P2 to Hobart (using a Fe/P ratio of 0.47 mmol/mol [*Parekh et al.*, 2005] (Figure 2d)), indicating that upper waters (down to ~100–200 m) between 43 and 47°S to the southeast of Tasmania were iron-replete whereas all other regions along this section were iron-deficient. Fe*(P) was lowest (−0.75) in the pycnocline at P2 (PF), indicating iron limitation. Here, low light at the base of the mixed layer may exacerbate iron limitation since the cellular iron demand increases under low light (and low silicic acid in the case of diatoms) conditions [*Hoffmann et al.*, 2008].

[18] Clearly the tracer Fe* is highly dependant on the Fe/P or Fe/Si ratios, which will vary meridionally and depend on the resident phytoplankton community, light, differential nutrient supply and the degree of iron limitation [*Sunda and Huntsman*, 1995], and are likely to tend to higher values in high-iron environments [*Twining et al.*, 2004]. However, in a qualitative sense, Fe* does demonstrate well the broad-scale spatial differences in iron limitation and supply which are consistent with our Fe/NO_x ratios calculated above. Interestingly, the application of the Fe*(Si) along the same transect (using Fe/Si = 0.92 mmol/mol, which is the mean elemental ratio of plankton in nonfertilized waters during SoFeX) [*Twining et al.*, 2004], indicates that the majority of the region is iron-deficient, with only surface waters (0–25 m) around 45°S being iron sufficient, and demonstrating Fe-Si colimitation across the northern SAZ.

3.4. Atmospheric Iron and Aluminum Concentrations and Deposition Fluxes

[19] Aluminum concentrations for aerosol samples AeroSAZ-1 and AeroSAZ-8 (which were collected at the most northerly sections at the start and end of the cruise; Figure S1) were significantly higher than for the other 6 samples, with an average concentration of 58 ± 4 ng m^{-3} (n = 2) compared to an average of 23 ± 22 ng m^{-3} (n = 8) for the entire sample set (Table S1). Excluding both high concentration samples yields a lower average value of 12 ± 7 ng m^{-3} (n = 6), which may be more representative of the broader Southern Ocean. Iron concentrations ranged from 17.0 ± 7.0 (sample AeroSAZ-4) to 5.0 ± 1.6 ng m^{-3} (sample AeroSAZ-6), but were not significantly correlated to aluminum concentrations (Table S1). Crustal and marine enrichment factors calculated independently (using aluminum and sodium data, respectively) allow us to estimate the deviation of the composition of an element from its sources [*Duce et al.*, 1983]. For iron, the crustal enrichment factors were close to 1 whereas the marine enrichment factors were close to 1000, clearly indicating a crustal origin of the transported iron. Our data do not indicate that there is greater dust deposition in the eastern sector of the study area (Table S1), even if atmospheric circulation patterns and model simulations [*Mahowald et al.*, 2005] suggest preferential transport from the Australian continent [*Ekstrom et al.*, 2004]. A clear latitudinal trend of decreasing dust concentrations can be observed in this region, with ~2 μg m^{-3} dust concentration reported in austral summer at Cape Grim (~41°S) [*Ginoux et al.*, 2004], a mean value of 0.75 μg m^{-3} for samples AeroSAZ-1 and AeroSAZ-8 (~43–46.5°S), and finally a mean concentration of 0.15 μg m^{-3} for the other samples (south of ~46.5°S).

3.5. Solubility of the Transported Iron

[20] Iron solubility values for each sample are reported in Table S1 as the sum of two leaches. Since the first leach contained >80% of the iron that dissolved in both leaches, we assume that two leaches are sufficient to determine the amount of "instantaneous soluble iron," consistent with the study by *Buck et al.* [2006]. Dissolution values ranged from 0.2 to 2.5% for samples AeroSAZ-1 to AeroSAZ-7, which is in a range that is commonly accepted for mineral dust samples [e.g., *Bonnet and Guieu*, 2004]. For sample AeroSAZ-8, the iron solubility was significantly higher with a value of 17.7%. This aerosol sample may have included particles emitted from biomass burning. The OMI Aerosol Index on the 18 January 2007 (when the sample was collected) indicated a smoke patch over southern Tasmania, and the MODIS satellite sensors detected several fires in Tasmania at that time (Figure S4). Higher iron solubility in biomass combustion particles has been suggested in former studies [*Guieu et al.*, 2005].

3.6. Deposition Fluxes of Dust and Total Iron

[21] For this study, we estimated the deposition flux of total and soluble iron for each of the three process stations from the samples collected when visiting (and on transects to and from) the stations (Tables 1 and S2) and were determined following calculations described by *Wagener et al.* [2008]. Dry fluxes were calculated by applying a deposition velocity to the dust concentration. In order to estimate deposition velocities, a range of median mass diameters (2.5–6.5 μm) [*Knight et al.*, 1995; *Wagener et al.*, 2008] and a surface wind speed of 20 ± 10 knots (based on the average shipboard wind measurements) were used. Wet deposition was estimated from a range of scavenging ratios (200 ± 100). The range of precipitation data (2 ± 1 mm d^{-1}) was based on daily 1° precipitation estimates for the study period from the Global Precipitation Climatology Project [*Adler et al.*, 2003]. Total iron deposition was calculated from the total iron concentrations measured and dFe fluxes estimated from our solubilities derived from dissolution experiments.

[22] Since both air mass back trajectory calculations and chemical concentration data for aerosol iron and aluminum

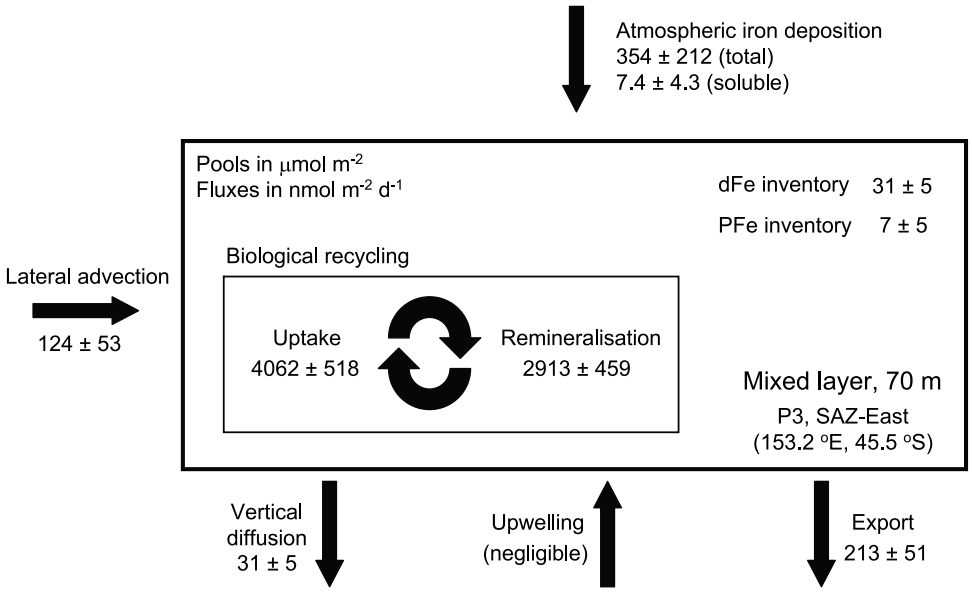

Figure 4. A biogeochemical iron budget for the surface mixed layer at SAZ-Sense process station P3 (SAZ-East). Pools are given in μmol m^{-2} and fluxes in nmol m^{-2} d^{-1}. The mean and standard deviation (1 standard deviation) are given. The fluxes associated with "recycled" iron are significantly greater than "new" iron and export fluxes. Iron remineralization rates have been multiplied by three to take into account the likely effects of bacterivory and herbivory [*Strzepek et al.*, 2005]. Note the uncertainties on each flux estimate, which may account for the "missing" iron required to balance the budget.

indicated that there was a clear difference between samples collected in the north (AeroSAZ-1 and 8) and samples collected in the south (AeroSAZ-2 to 7), we assume that mean values of samples AeroSAZ-2 to AeroSAZ-7 are the first best estimates of mineral dust fluxes over this part of the open Southern Ocean. Our estimated fluxes of mineral dust (0.37 ± 0.18 mg m^{-2} d^{-1}) are in good agreement with the earlier study of *Duce et al.* [1991] (0.27 mg m^{-2} d^{-1}), but are generally lower than climatological dust models (1.12 mg m^{-2} d^{-1} [*Mahowald et al.*, 2005]; 2.47 mg m^{-2} d^{-1} [*Luo et al.*, 2003]) for the region. This confirms the overestimation by such global dust models (usually parameterized for Northern Hemisphere conditions) [*Boyd and Mackie*, 2008] for dust deposition over oceanic regions of the Southern Hemisphere [*Wagener et al.*, 2008].

[23] The atmospheric deposition term is subject to significant uncertainties because it is based on one or two aerosol samples collected over one or two days during the studied process stations. As dust deposition is a highly episodic phenomenon, the sampling timescale is clearly insufficient for seasonal budgets estimations. However, despite this caveat, estimation of total iron aerosol deposition fluxes are in good agreement with the other budget terms (Table 1), and our mean total dust deposition predictions for the open Southern Ocean are consistent with previous observed estimates [*McGowan et al.*, 2005; *Mackie at al.*, 2008]. Our total atmospheric iron fluxes (and dFe fluxes based on aerosol quasi-instantaneous dissolution experiments) coupled with oceanic dFe supply are insufficient to sustain the biological iron requirements (Table 1 and Figure 4). The use of a short-term "abiotic" aerosol leaching protocol for solubility estimates could largely underestimate the fraction of iron that dissolves in the oceanic mixed layer, thus clearly highlighting the need of a better comprehension of the longer-term release of iron from atmospheric particles in the surface ocean (possibly driven by microbes, siderophores or photochemistry) that will increase the aerosol iron contribution to the inventory of dFe in the mixed layer.

3.7. Downward Particulate Metal Export

[24] Trace metal export fluxes at 150 m depth were calculated from the mean of four separate collection cups deployed on a free-floating sediment trap, each of which were opened for 12 h periods during each process station occupation. We observed significantly greater iron export fluxes at our two northern SAZ stations (P1 and P3) compared to our PF site (P2) (Table 1). The downward pFe flux varied between 69 (PF) to 213 (SAZ-East) nmol m^{-2} d^{-1}, and was by far the most significant loss term for iron from the mixed layer (Table 1). The daily export flux represents between 1 and 3% of the pFe inventory in the mixed layer, which represents a turnover time of the pFe pool of around 33–100 days. The turnover time is likely an underestimate by ~30% due to the fraction of lithogenic material in suspended and sinking particles which we do not recover (e.g., *Frew et al.* [2006] report a lithogenic-to-total pFe fraction of 36–50% in sinking particles and near 90% in suspended particles; also see section 2). The Fe/C molar ratio in sinking exported particles intercepted by the sediment traps varied from 33 μmol/mol at P2 (PF) to 50 μmol/mol at P1 (SAZ-West), but was much larger at 248 μmol/mol at P3 (SAZ-East). These values are similar to the results reported by *Frew et al.* [2006] during FeCycle (178–217 μmol/mol). The Fe/C sinking export ratios were of

similar magnitude to those of suspended mixed layer particles at P1 and P2 (40 and 55 μmol/mol, respectively; Table 1), but significantly greater than those of suspended particles at P3 (32 μmol/mol). This indicates the preferential remineralization of carbon relative to iron in the SAZ-East, most likely due to scavenging of remineralized iron by sinking particles and solubilization of organic carbon with depth [*Frew et al.*, 2006], which may be related to higher temperatures at this location. Interestingly, Fe/C ratios using our four different estimates (consumption inferred from dissolved nutrient depletion, phytoplankton radiotracer uptake, suspended particle concentrations, and sinking particle concentrations) tend to follow the published global pattern of Fe/C ratios shown by *Boyd et al.* [2007, Figure 3] for low-iron HNLC waters. There remains, however, some uncertainty when comparing Fe/C ratios obtained by different methods due to artifacts associated with sampling and analysis (e.g., timescales of integration, where dissolved nutrient budgets will integrate over longer periods than uptake studies).

3.8. Construction of Biogeochemical Iron Budgets

[25] The measured iron pools and fluxes during SAZ-Sense enable us to construct mixed layer pelagic iron budgets for each of our three process stations in subantarctic and polar frontal regions, and to estimate the main sources, sinks and biological cycling of iron. There have been few previous attempts to construct biogeochemical iron budgets based on field observations in low-iron [*Price and Morel*, 1998] or high-iron [*Bowie et al.*, 2001] systems, and earlier studies have tended to focus on either geochemical or biological components independently. An earlier iron budget based on the FeCycle experiment, conducted within a mesoscale SF_6-labeled patch, highlighted the importance of biological iron recycling and the relative contribution of new versus recycled iron [*Boyd et al.*, 2005], although did not contain any field observations of atmospheric iron deposition. Our SAZ-Sense data are presented in Table 1 for all three sites, and a biogeochemical iron budget for the surface mixed layer at P3 (SAZ-East) is shown in Figure 4. The following trends are evident.

[26] First, the dominant "new" iron fluxes in our summertime budgets are generally particulate iron associated with the flux of atmospheric dust and downward export. "New" iron supplied to P1 and P3 is of a similar magnitude and significantly greater than that at P2. Atmospheric iron deposition is the dominant total supply term at P1 and P2 (4–7 fold greater than the sum of oceanic supply terms), but the oceanic (lateral advective) supply term at P3 is relatively more important (35% of the atmospheric flux). If we compare dFe fluxes using solubility estimates, oceanic fluxes dominate the "new" iron terms. Second, atmospheric iron depositional fluxes are greater than, but broadly comparable, to downward pFe export fluxes, and both terms tend to decrease southward, indicating a tight coupling between these supply and loss terms in both low-iron and high-iron ecosystems. Third, Fe/C cellular uptake ratios are of a similar order of magnitude to those in suspended mixed layer and exported particles, except at P3 where the Fe/C export term is 3–8 fold greater (indicative of the decoupling of Fe, N and C cycles in the SAZ-East). The relative difference between Fe/C in suspended (mixed layer) and sinking (exported) particles (which varies with location) may indicate differences in the remineralization length scales, and export transfer efficiencies of carbon relative to iron among the different particles [*Lamborg et al.*, 2008]. This has important implications for effectiveness of stimulation of the biological pump by increased ocean iron fertilization in HNLC regions in the absence of "new" iron sources (e.g., dust or sediments). Fourthly, the short-term (days-weeks) iron fluxes within the "ferrous wheel" [*Kirchman*, 1996] in our summertime budget are dominated by biological uptake and remineralization ("recycled" iron), and are significantly larger (6–11 fold at P1, 2–5 fold at P2, and 6–9 fold at P3) than the long-term (months), seasonal "new" iron fluxes supplied by atmospheric and oceanic sources, consistent with the FeCycle observations [*Boyd et al.*, 2005]. The rate of iron remineralization accounts for up to 70% of the iron uptake (Figure 4), highlighting the additional need for "new" iron sources, as observed during KEOPS [*Sarthou et al.*, 2008].

[27] The observed SAZ-Sense iron fluxes for the three process stations indicate that biological iron demand cannot be satisfied by the "new" iron supply, with an additional iron supply of the order of 744 to 1836 nmol m^{-2} d^{-1} required, of similar magnitude to that observed during FeCycle (851 nmol m^{-2} d^{-1}) [*Boyd et al.*, 2005]. This observation is consistent with the observation that our estimated new primary production based on biological uptake of "new" iron is significantly (8–20 fold) lower than the measured gross primary production at the three process stations during the expedition (Table 1). Iron fluxes in our biogeochemical budgets are clearly dominated by short-term uptake and remineralization, and it is evident that our estimated uncertainties on these processes could easily account for the "missing" iron terms. Moreover, atmospheric deposition (wet and dry) and lateral advective supply of iron are both episodic, which may not have been sampled during our process station observation periods, and horizontal supply of dissolved iron from UCDW upwelled in winter south of the SAZ may dominate fluxes on annual timescales. Clearly, the iron flux processes shown in Figure 4 are based on different timescales (short-term, daily, seasonal, annual), which indicates that no short-term balance of our iron budgets is required.

[28] We estimate an *f*e ratio for our three process stations from "uptake of new iron/uptake of new + regenerated iron," and an F*e* ratio from "biogenic pFe export/uptake of new + regenerated iron," following *Boyd et al.* [2005]. Our *f*e ratios vary from 0.06 to 0.16 and were inversely correlated to the iron inventories (i.e., lower in the northern SAZ at P1 and P3, and higher in the PF at P2), and F*e* ratios vary from 0.03 to 0.05. Both our *f*e and F*e* ratios are comparable with those calculated for FeCycle (*f*e = 0.17 and F*e* = 0.09) *Boyd et al.* [2005]. The SAZ-Sense *f*e ratios are lower than the *f* ratio for the SAZ/PFZ during spring ($\sim$0.5) [*Savoye et al.*, 2004] and summer ($\leq$0.3, this study) (A.-J. Cavagna, personal communication, 2009). This indicates widespread iron limitation in these waters and highlights that the fluxes of "recycled" iron (uptake and remineralization) within the ferrous wheel are significantly greater (and are turned over

more rapidly) than the fluxes of "new" iron. There is clearly a need for further refinement of the cycling of iron within the biogenic particulate pools to investigate the tight coupling between uptake and remineralization, and to understand where additional "new" iron supply originates from in pelagic ecosystems where the biogeochemical cycling of iron is dominated by the biota.

4. Conclusions

[29] The SAZ-Sense expedition provided an ideal natural laboratory to study iron-driven elevated production and biomass in differing water masses (subantarctic and polar frontal regions) of the Southern Ocean. The seasonal biomass and production observations in the PFZ/PF contrast with those in the northern SAZ/STF, which implicates alternative supply terms for iron into the northern and southern subantarctic regions. In addition, comparison of subantarctic regions southeast and southwest of Tasmania has demonstrated a natural gradient of iron fertilization of the Southern Ocean which will be important for examining future climate-driven changes in iron supply and production in the region, as well as in the greater circumpolar SAZ.

[30] At our PF station, we observed a close coupling between iron and nutrients dynamics, where other iron supply terms (advection, atmospheric deposition) were lower. Previously, *Moore et al.* [1999] have suggested that topography destabilizes the deep-reaching flow of the Antarctic Circumpolar Current, leading to the formation of mesoscale eddies and meanders which drive upwelling supply of iron to surface waters. *Sokolov and Rintoul* [2007] have further suggested that blooms along the Southern Ocean fronts are generally initiated by upwelling of a limiting nutrient (presumably iron) where the flow crosses bathymetric features, and the system appears to retain iron efficiently, allowing the bloom to persist for long distances (up to 2000 km) downstream of the iron source. Our data indicates that the delivery of iron-enriched deep waters by convective mixing and upwelling does relieve iron limitation and support a deep chlorophyll maximum in the PF.

[31] Our budgets reveal very different iron supply and loss terms in northern SAZ compared to the southern SAZ and PF waters, with inherent differences between iron and nutrients dynamics in northern SAZ waters. Here, the short-term (weeks-months) iron supply decouples the full seasonal major nutrient cycles of convective mixing, uptake and remineralization which results in elevated winter reserves and summer minima in surface waters. *Ellwood et al.* [2008] suggested that the main supply of dissolved iron into the SAZ during winter is via Ekman transport of waters from the south, although their cruise track was further offshore and hence they may have missed iron supplied from the continental shelf. Our calculations indicate that atmospheric supply (despite the large uncertainties in this term) and Ekman-driven lateral advection from the south cannot supply enough iron to fuel the strong spring-summer blooms within the frontal regions of the northern SAZ. Our data indicate for the first time an important source of iron to surface waters in the northern SAZ and STF (particularly to the southeast of Australia) during summer. This results from a combination of shelf sedimentary iron transported laterally and to the south (via the EAC extension) over long distances (up to 1000 km) in subsurface waters, and iron dust and/or bushfire smoke supplied off the Australian continent in summer (both directly to the region, and deposited further north and advected south). Although inputs of continental margin iron [*Lam and Bishop*, 2008] have been shown to be transported offshore in mesoscale eddies [*Johnson et al.*, 2005] in the north Pacific Ocean, our observations are the first for Southern Ocean waters. Similar iron supply processes will likely drive global biogeochemical cycles more broadly in the wider circumpolar Southern Ocean. The interaction of local eddies of the EAC extension with the continental shelf-edge (where iron is entrained) are important for resolving the fine-scale structure in dissolved and particulate iron distributions in the region. The interleaving of warm, salty, iron-enriched subtropical waters over cooler, fresher, HNLC SAZ waters supports the elevated, yet variable biomass and productivity observed in this sector of the SAZ during spring and summer.

[32] The atmospheric depositional term in our budgets may be the most difficult to constrain seasonally and annually (it is based on sparse number of observations), clearly pointing to the need for time series observations at land-based sites and on ship's of opportunity operating in waters to the south and east of Australia. In addition, we also clearly require a better understanding of the solubility, residence time and bioavailability of iron in dust and sedimentary particles. Our dissolved and particulate iron observations (especially at depth), together with Fe/C uptake and export data, will have important implications for global ocean biogeochemical models, which clearly need to focus on the importance of recycled versus new Fe.

[33] The SAZ-Sense observations have important longer-term climatic implications for the productivity of the Southern Ocean for several reasons. First, the frequency and scale of dust emissions (e.g., from Australia) are predicted to increase with future changes in regional climate [*IPCC*, 2007], although how ocean biogeochemical cycles respond on the global scale is uncertain [*Tagliabue et al.*, 2008]. Second, the importance of the EAC (and similar western boundary currents) may increase in coming decades as atmospheric and ocean circulation changes driven by climate warming cause the SAZ to experience greater advective inputs from the subtropical gyres [*Ridgway and Dunn*, 2007; *Hill et al.*, 2008], resulting in the penetration of iron-enriched waters deeper south into the SAZ [*Ridgway*, 2007a]. Third, since overturning circulation is expected to weaken with changes in climate resulting in increased stratification and less delivery of nutrients such as iron from below, boundary fluxes of sedimentary iron may become increasingly more important for future Southern Ocean productivity [*Tagliabue et al.*, 2009]. Our study has also highlighted the complexity of the biogeochemical cycling of iron in dynamic oceanographic regions which are naturally fertilized with this essential trace element through multiple sources such as atmospheric dusts and continental sediments, and demonstrated the need for high resolution data sets over seasonal timescales. Additional regional process studies are necessary to inform interna-

tional trace metal programs such as GEOTRACES (www.geotraces.org) which are focused on global ocean sections.

[34] **Acknowledgments.** We would like to thank the captain, officers, and crew of the RSV *Aurora Australis* for all their support during SAZ-Sense. We are grateful to Mark Rosenberg and the hydrography team for provision of CTD data, Neil Johnson and Alicia Navidad for nutrients analysis, Alan Poole and Aaron Spurr for technical support, Rémi Losno for assistance in aerosol analysis, Mathieu Mongin for tracer release model simulations, and Karen Westwood for gross primary productivity data. Thanks to Brian Griffiths, Doug Mackie, Richard Matear, Klaus Meiners, and Alessandro Tagliabue for providing useful comments on the manuscript. The NERC Earth Observation Data Acquisition and Analysis Service (NEODAAS) provided the remote sensing data in Figure 1, the NASA-Goddard Space Flight Centre–Ozone Processing Team provided daily data of OMI Aerosol Index, and the NOAA Air Resource Laboratory (ARL) provided the HYSPLIT model. D.L. was supported by a travel grant from the Belgian Belcanto (Belgian research on Carbon uptake in the Antarctic Ocean) project and a BePoles fellowship from the International Polar Foundation. T.W. was supported by a BDI grant from CNRS and Région PACA, by CNRS PICS project 3604, and by the "Soutien à la mer" CSOA CNRS-INSU. P.W.B. was supported by the New Zealand FRST Coasts and Oceans OBI. This research was supported by the Australian Government Cooperative Research Centres Programme through the Antarctic Climate and Ecosystems CRC (ACE CRC) and Australian Antarctic Science project 2720.

References

Adler, R. F., et al. (2003), The version-2 global precipitation climatology project (GPCP) monthly precipitation analysis (1979–present), *J. Hydrometeorol.*, *4*(6), 1147–1167, doi:10.1175/1525-7541(2003)004<1147:TVGPCP>2.0.CO;2.

Blain, S., et al. (2007), Effect of natural iron fertilization on carbon sequestration in the Southern Ocean, *Nature*, *446*, 1070–1074, doi:10.1038/nature05700.

Blain, S., S. Bonnet, and C. Guieu (2008), Dissolved iron distribution in the tropical and subtropical southeastern Pacific, *Biogeosciences*, *5*(1), 269–280.

Bonnet, S., and C. Guieu (2004), Dissolution of atmospheric iron in seawater, *Geophys. Res. Lett.*, *31*, L03303, doi:10.1029/2003GL018423.

Bowie, A. R., and M. C. Lohan (2009), Analysis of iron in seawater, in *Practical Guidelines for the Analysis of Seawater*, edited by O. Wurl, chap. 12, pp. 235–257, Taylor and Francis, Boca Raton, Fla., ISBN:978-1-4200-7306-5.

Bowie, A. R., et al. (2001), The fate of added iron during a mesoscale fertilisation experiment in the Southern Ocean, *Deep Sea Res., Part II*, *48*, 2703–2743, doi:10.1016/S0967-0645(01)00015-7.

Bowie, A. R., P. N. Sedwick, and P. J. Worsfold (2004), Analytical intercomparison between flow injection-chemiluminescence and flow injection-spectrophotometry for the determination of picomolar concentrations of iron in seawater, *Limnol. Oceanogr. Methods*, *2*, 42–54.

Boyd, P. W., and D. Mackie (2008), Comment on the Southern Ocean biological response to aeolian iron deposition, *Science*, *319*, 159a, doi:10.1126/science.1149884.

Boyd, P. W., et al. (1999), Role of iron, light, and silicate in controlling algal biomass in subantarctic waters SE of New Zealand, *J. Geophys. Res.*, *104*, 13,395–13,408, doi:10.1029/1999JC900009.

Boyd, P. W., et al. (2000), A mesoscale phytoplankton bloom in the polar Southern Ocean stimulated by iron fertilization, *Nature*, *407*, 695–702, doi:10.1038/35037500.

Boyd, P. W., et al. (2004), Episodic enhancement of phytoplankton stocks in New Zealand subantarctic waters: Contribution of atmospheric and oceanic iron supply, *Global Biogeochem. Cycles*, *18*, GB1029, doi:10.1029/2002GB002020.

Boyd, P. W., et al. (2005), FeCycle: Attempting an iron biogeochemical budget from a mesoscale SF6 tracer experiment in unperturbed low iron waters, *Global Biogeochem. Cycles*, *19*, GB4S20, doi:10.1029/2005GB002494.

Boyd, P. W., et al. (2007), Mesoscale iron enrichment experiments 1993–2005: Synthesis and future directions, *Science*, *315*, 612–617, doi:10.1126/science.1131669.

Buck, C. S., W. M. Landing, J. A. Resing, and G. T. Lebon (2006), Aerosol iron and aluminum solubility in the northwest Pacific Ocean: Results from the 2002 IOC cruise, *Geochem. Geophys. Geosyst.*, *7*, Q04M07, doi:10.1029/2005GC000977.

Cassar, N., M. L. Bender, B. A. Barnett, S. Fan, W. J. Moxim, H. Levy, and B. Tilbrook (2007), The Southern Ocean biological response to aeolian iron deposition, *Science*, *317*, 1067–1070, doi:10.1126/science.1144602.

Cassar, N., M. L. Bender, B. A. Barnett, S. Fan, W. J. Moxim, H. Levy, and B. Tilbrook (2008), Response to comment on the Southern Ocean biological response to aeolian iron deposition, *Science*, *319*, 159b, doi:10.1126/science.1150011.

Coale, K. H., R. M. Gordon, and X. J. Wang (2005), The distribution and behaviour of dissolved and particulate iron and zinc in the Ross Sea and Antarctic Circumpolar Current along 170 degrees W, *Deep Sea Res., Part I*, *52*, 295–318, doi:10.1016/j.dsr.2004.09.008.

Croot, P. L., et al. (2007), Physical mixing effects on iron biogeochemical cycling: FeCycle experiment, *J. Geophys. Res.*, *112*, C06015, doi:10.1029/2006JC003748.

de Baar, H. J. W., et al. (1995), Importance of iron for plankton blooms and carbon-dioxide drawdown in the Southern Ocean, *Nature*, *373*, 412–415, doi:10.1038/373412a0.

de Baar, H. J. W., L. J. A. Gerringa, P. Laan, and K. R. Timmermans (2008), Efficiency of carbon removal per added iron in ocean iron fertilization, *Mar. Ecol. Prog. Ser.*, *364*, 269–282, doi:10.3354/meps07548.

Duce, R. A., R. Arimoto, B. J. Ray, C. K. Unni, and P. J. Harder (1983), Atmospheric trace elements at Enewetak Atoll: I. Concentrations, sources, and temporal variability, *J. Geophys. Res.*, *88*(C9), 5321–5342, doi:10.1029/JC088iC09p05321.

Duce, R., et al. (1991), The atmospheric input of trace species to the world ocean, *Global Biogeochem. Cycles*, *5*(3), 193–259, doi:10.1029/91GB01778.

Ekstrom, M., G. H. McTainsh, and A. Chappell (2004), Australian dust storms: Temporal trends and relationships with synoptic pressure distributions (1960–99), *Int. J. Climatol.*, *24*, 1581–1599, doi:10.1002/joc.1072.

Ellwood, M. J., P. W. Boyd, and P. Sutton (2008), Winter-time dissolved iron and nutrient distributions in the subantarctic zone from 40–52S; 155–160E, *Geophys. Res. Lett.*, *35*, L11604, doi:10.1029/2008GL033699.

Fitzwater, S. E., K. S. Johnson, R. M. Gordon, K. H. Coale, and W. O. Smith (2000), Trace metal concentrations in the Ross Sea and their relationship with nutrients and phytoplankton growth, *Deep Sea Res., Part II*, *47*, 3159–3179, doi:10.1016/S0967-0645(00)00063-1.

Frew, R. D., et al. (2006), Particulate iron dynamics during FeCycle in subantarctic waters southeast of New Zealand, *Global Biogeochem. Cycles*, *20*, GB1S93, doi:10.1029/2005GB002558.

Ginoux, P., J. M. Prospero, O. Torres, and M. Chin (2004), Long-term simulation of global dust distribution with the GOCART model: Correlation with North Atlantic Oscillation, *Environ. Model. Softw.*, *19*(2), 113–128, doi:10.1016/S1364-8152(03)00114-2.

Gruber, N., and J. L. Sarmiento (1997), Global patterns of marine nitrogen fixation and denitrification, *Global Biogeochem. Cycles*, *11*, 235–266, doi:10.1029/97GB00077.

Guieu, C., S. Bonnet, T. Wagener, and M. D. Loye-Pilot (2005), Biomass burning as a source of dissolved iron to the open ocean?, *Geophys. Res. Lett.*, *32*(19), L19608, doi:10.1029/2005GL022962.

Hesse, P. P. (1994), The record of continental dust from Australia in Tasman Sea Sediments, *Quat. Sci. Rev.*, *13*(3), 257–272, doi:10.1016/0277-3791(94)90029-9.

Hill, K. L., S. R. Rintoul, R. Coleman, and K. R. Ridgway (2008), Wind forced low frequency variability of the East Australia Current, *Geophys. Res. Lett.*, *35*, L08602, doi:10.1029/2007GL032912.

Hoffmann, L. J., I. Peeken, and K. Lochte (2008), Iron, silicates and light co-limitation of three Southern Ocean diatom species, *Polar Biol.*, *31*, 1067–1080, doi:10.1007/s00300-008-0448-6.

Ibisanmi, E. B., K. A. Hunter, S. Sander, P. W. Boyd, and A. R. Bowie (2009), Vertical distributions of iron- (III) complexing ligands in the Southern Ocean, *Deep Sea Res., Part II*, in press.

IPCC (2007), *Climate Change 2007: The Physical Science Basis. Contribution of Working Group 1 to the Fourth Assessment Report of the Intergovernmental Panel on Climate Change*, edited by S. Solomon et al., Intergov. Panel on Clim. Change, Cambridge, New York.

Johnson, K. S., R. M. Gordon, and K. H. Coale (1997), What controls dissolved iron concentrations in the world ocean?, *Mar. Chem.*, *57*, 137–161, doi:10.1016/S0304-4203(97)00043-1.

Johnson, W. K., L. A. Miller, N. E. Sutherland, and C. S. Wong (2005), Iron transport by mesoscale Haida eddies in the Gulf of Alaska, *Deep Sea Res., Part II*, *52*, 933–953, doi:10.1016/j.dsr2.2004.08.017.

Kirchman, D. L. (1996), Microbial ferrous wheel, *Nature*, *383*, 303–304, doi:10.1038/383303a0.

Knight, A., G. McTainsh, and R. Simpson (1995), Sediment loads in an Australian dust storm: Implications for present and past dust processes, *Catena*, *24*(3), 195–213, doi:10.1016/0341-8162(95)00026-O.

Lam, P. J., and J. K. B. Bishop (2008), The continental margin is a key source of iron to the HNLC North Pacific Ocean, *Geophys. Res. Lett.*, *35*, L07608, doi:10.1029/2008GL033294.

Lamborg, C. H., K. O. Buesseler, and P. J. Lam (2008), Sinking fluxes of minor and trace elements in the North Pacific Ocean measured during the VERTIGO program, *Deep Sea Res., Part II*, *55*, 1564–1577, doi:10.1016/j.dsr2.2008.04.012.

Lannuzel, D., et al. (2009), Distributions of dissolved and particulate iron in the subantarctic and polar frontal Southern Ocean (Australian sector), *Deep Sea Res., Part II*, in press.

Lourey, M. J., and T. W. Trull (2001), Seasonal nutrient depletion and carbon export in the subantarctic and polar frontal zones of the Southern Ocean south of Australia, *J. Geophys. Res.*, *106*(C12), 31,463–31,487, doi:10.1029/2000JC000287.

Luo, C., N. M. Mahowald, and J. del Corral (2003), Sensitivity study of meteorological parameters on mineral aerosol mobilization, transport, and distribution, *J. Geophys. Res.*, *108*(D15), 4447, doi:10.1029/2003JD003483.

Luo, C., N. Mahowald, T. Bond, P. Y. Chuang, P. Artaxo, R. Siefert, Y. Chen, and J. Schauer (2008), Combustion iron distribution and deposition, *Global Biogeochem. Cycles*, *22*, GB1012, doi:10.1029/2007GB002964.

Mackie, D., P. Boyd, G. Mc Tainsh, N. W. Tindale, T. Westberry, and K. Hunter (2008), Biogeochemistry of iron in Australian dust: From eolian uplift to marine uptake, *Geochem. Geophys. Geosyst.*, *9*, Q03Q08, doi:10.1029/2007GC001813.

Mahowald, N. M., et al. (2005), Atmospheric global dust cycle and iron inputs to the ocean, *Global Biogeochem. Cycles*, *19*, GB4025, doi:10.1029/2004GB002402.

Maldonado, M. T., and N. M. Price (1996), Influence of N substrate on Fe requirements of marine centric diatoms, *Mar. Ecol. Prog. Ser.*, *141*, 161–172, doi:10.3354/meps141161.

Martin, J. H., R. M. Gordon, S. Fitzwater, and W. W. Broenkow (1989), VERTEX: Phytoplankton/iron studies in the Gulf of Alaska, *Deep Sea Res., Part A*, *36*, 649–680.

McGowan, H. A., B. Kamber, G. H. McTainsh, and S. K. Marx (2005), High resolution provenancing of long travelled dust deposited on the Southern Alps, New Zealand, *Geomorphology*, *69*, 208–221, doi:10.1016/j.geomorph.2005.01.005.

Metzl, N., B. Tilbrook, and A. Poisson (1999), The annual fCO_2 cycle and the air-sea CO_2 flux in the sub-Antarctic Ocean, *Tellus, Ser. B*, *51*, 849–861, doi:10.1034/j.1600-0889.1999.t01-3-00008.x.

Moore, J. K., and O. Braucher (2008), Sedimentary and mineral dust sources of dissolved iron to the world ocean, *Biogeosciences*, *5*, 631–656.

Moore, J., et al. (1999), SeaWiFS satellite ocean color data from the Southern Ocean, *Geophys. Res. Lett.*, *26*(10), 1465–1468, doi:10.1029/1999GL900242.

Parekh, P., M. J. Follows, and E. A. Boyle (2005), Decoupling of iron and phosphate in the global ocean, *Global Biogeochem. Cycles*, *19*, GB2020, doi:10.1029/2004GB002280.

Pearce, I., A. T. Davidson, P. G. Thomson, S. Wright, and R. van den Enden (2009), Marine microbial ecology in the subantarctic zone: Rates of bacterial and phytoplankton growth and grazing by heterotrophic protists, *Deep Sea Res., Part II*, in press.

Price, N. M., and F. M. M. Morel (1998), Biological cycling of iron in the ocean, in *Metal Ions in Biological Systems, vol. 35, Iron Transport and Storage in Microorganisms, Plants and Animals*, edited by A. Sigel and H. Sigel, pp. 1–36, Marcel Dekker, New York.

Ridgway, K. R. (2007a), Long-term trend and decadal variability of the southward penetration of the East Australian Current, *Geophys. Res. Lett.*, *34*, L13613, doi:10.1029/2007GL030393.

Ridgway, K. R. (2007b), Seasonal circulation around Tasmania: An interface between eastern and western boundary dynamics, *J. Geophys. Res.*, *112*, C10016, doi:10.1029/2006JC003898.

Ridgway, K. R., and J. R. Dunn (2007), Observational evidence for a Southern Hemisphere oceanic supergyre, *Geophys. Res. Lett.*, *34*, L13612, doi:10.1029/2007GL030392.

Rintoul, S. R., and J. L. Bullister (1999), A late winter hydrographic section from Tasmania to Antarctica, *Deep Sea Res., Part I*, *46*, 1417–1454, doi:10.1016/S0967-0637(99)00013-8.

Rintoul, S. R., and T. W. Trull (2001), Seasonal evolution of the mixed layer in the subantarctic zone south of Australia, *J. Geophys. Res.*, *106*, 31,447–31,462, doi:10.1029/2000JC000329.

Sarthou, G., et al. (1997), Fe and H_2O_2 distributions in the upper water column in the Indian sector of the Southern Ocean, *Earth Planet. Sci. Lett.*, *147*, 83–92, doi:10.1016/S0012-821X(97)00004-6.

Sarthou, G., et al. (2008), The fate of biogenic iron during a phytoplankton bloom induced by natural fertilisation: Impact of copepod grazing, *Deep Sea Res., Part II*, *55*, 734–751, doi:10.1016/j.dsr2.2007.12.033.

Savoye, N., F. Dehairs, M. Elskens, D. Cardinal, E. E. Kopczyńska, T. W. Trull, S. Wright, W. Baeyens, and F. B. Griffiths (2004), Regional variation of spring N-uptake and new production in the Southern Ocean, *Geophys. Res. Lett.*, *31*, L03301, doi:10.1029/2003GL018946.

Schroth, A. W., J. Crusius, E. R. Sholkovitz, and B. C. Bostick (2009), Iron solubility driven by speciation in dust sources to the ocean, *Nat. Geosci.*, *2*, 337–340, doi:10.1038/ngeo501.

Sedwick, P. N., et al. (1997), Iron and manganese in surface waters of the Australian subantarctic region, *Deep Sea Res., Part I*, *44*, 1239–1253, doi:10.1016/S0967-0637(97)00021-6.

Sedwick, P. N., et al. (1999), Limitation of algal growth by iron deficiency in the Australian subantarctic region, *Geophys. Res. Lett.*, *26*, 2865–2868, doi:10.1029/1998GL002284.

Sedwick, P. N., A. R. Bowie, and T. W. Trull (2008), Dissolved iron in the Australian sector of the Southern Ocean (CLIVAR-SR3 section): Meridional and seasonal trends, *Deep Sea Res., Part I*, *55*, 911–925, doi:10.1016/j.dsr.2008.03.011.

Sohrin, Y., et al. (2000), The distribution of Fe in the Australian sector of the Southern Ocean, *Deep Sea Res., Part I*, *47*, 55–84, doi:10.1016/S0967-0637(99)00049-7.

Sokolov, S., and S. R. Rintoul (2003), Subsurface structure of interannual temperature anomalies in the Australian sector of the Southern Ocean, *J. Geophys. Res.*, *108*(C9), 3285, doi:10.1029/2002JC001494.

Sokolov, S., and S. R. Rintoul (2007), On the relationship between fronts of the Antarctic Circumpolar Current and surface chlorophyll concentrations in the Southern Ocean, *J. Geophys. Res.*, *112*, C07030, doi:10.1029/2006JC004072.

Strzepek, R. F., et al. (2005), Spinning the "Ferrous Wheel": The importance of the microbial community in an iron budget during the FeCycle experiment, *Global Biogeochem. Cycles*, *19*, GB4S26, doi:10.1029/2005GB002490.

Sunda, W. G., and S. A. Huntsman (1995), Iron uptake and growth limitation in oceanic and coastal phytoplankton, *Mar. Chem.*, *50*, 189–206, doi:10.1016/0304-4203(95)00035-P.

Tagliabue, A., L. Bopp, and O. Aumont (2008), Ocean biogeochemistry exhibits contrasting responses to a large scale reduction in dust deposition, *Biogeosciences*, *5*, 11–24.

Tagliabue, A., L. Bopp, and O. Aumont (2009), Evaluating the importance of atmospheric and sedimentary iron sources to Southern Ocean biogeochemistry, *Geophys. Res. Lett.*, *36*, L13601, doi:10.1029/2009GL038914.

Trull, T., S. R. Rintoul, M. Hadfield, and E. R. Abraham (2001), Circulation and seasonal evolution of polar waters south of Australia: Implications for iron fertilization of the Southern Ocean, *Deep Sea Res., Part II*, *48*, 2439–2466, doi:10.1016/S0967-0645(01)00003-0.

Twining, B. S., S. B. Baines, N. S. Fisher, and M. R. Landry (2004), Cellular iron contents of plankton during the Southern Ocean Iron Experiment (SOFeX), *Deep Sea Res., Part I*, *51*, 1827–1850, doi:10.1016/j.dsr.2004.08.007.

Wagener, T., C. Guieu, R. Losno, S. Bonnet, and N. Mahowald (2008), Revisiting atmospheric dust export to the Southern Hemisphere ocean: Biogeochemical implications, *Global Biogeochem. Cycles*, *22*, GB2006, doi:10.1029/2007GB002984.

Watson, A. J., D. C. E. Bakker, A. J. Ridgwell, P. W. Boyd, and C. S. Law (2000), Effect of iron supply on Southern Ocean CO_2 uptake and implications for glacial atmospheric CO_2, *Nature*, *407*, 730–733, doi:10.1038/35037561.

A. R. Bowie, D. Lannuzel, T. A. Remenyi, and T. W. Trull, Antarctic Climate and Ecosystems CRC, University of Tasmania, Private Bag 80, Hobart, Tasmania 7001, Australia. (andrew.bowie@utas.edu.au)

P. W. Boyd, NIWA Centre for Chemical and Physical Oceanography, Department of Chemistry, University of Otago, Cumberland St., Dunedin 9014, New Zealand.

C. Guieu, Laboratoire d'Océanographie de Villefranche sur Mer, Université Pierre et Marie Curie, UMR 7093, CNRS, Caserne Nicolas, Quai de la Darse, BP 8, F-06238 Villefranche sur Mer, France.

P. J. Lam, Department of Marine Chemistry and Geochemistry, Woods Hole Oceanographic Institution, MS 25, 266 Woods Hole Rd., Woods Hole, MA 02543, USA.

A. T. Townsend, Central Science Laboratory, University of Tasmania, Private Bag 74, Hobart, Tasmania 7001, Australia.

T. Wagener, Marine Biogeochemie, Chemische Ozeanographie, Leibniz-Institut für Meereswissenschaften an der Universität Kiel, IFM-GEOMAR, Dienstgebäude Westufer, Düsternbrooker Weg 20, D-24105 Kiel, Germany.